International Journal of Engineering Research ISSN:2319-6890)(online),2347-5013(print)
Volume No.4, Issue No.6, pp : 315-320 01 June 2015

# Reinforced Sisal Fiber with Ferric Nitrate Composites

**Asif Jehan[1], Dr. Shirish Joshi[2] ,Dr. M.N. Bapat[3]**
[1, 2]Motilal Vigyan Mahavidhalya Bhopal (M.P.) India
[3] Regional Institute of Education Bhopal (M.P.) India
Email: - asifjehan14@gmail.com

***Abstract :Ferric oxide synthesized through annealing route. The present research work deals with ferrite composite prepared using chemical reactions. Ferric nitrates and ammonium chloride doped with sisal fiber has been prepared. The structural behavior of aluminum oxide was studied in XRD, SEM, TEM, FTIR & dielectric measurement. This behavior showed ferrite nature of the sample.***

**Key words: - $Fe_2O_3$, sintering method, XRD, TEM, SEM, FTIR and dielectric measurement**

## 1. Introduction

The present contemporaries of Physicists and Engineers are focusing to reduce the operation of traditional fillers and increase the utilization of bio waste natural fibre material [1]. The syntheses of polymer based on composite materials have opened new traditions for the polymer fabrication and have allowed the manufacture of new products with optimal properties and its special applications [2, 3]

Iron oxide particles with controlled size and shape have attracted great attention in the last years. Because of their unique properties, the iron oxides are used in a wide range of applications as gas sensors , catalysts or pigments [4-7].Due to their notable properties such biocompatibility and magnetism, iron oxides ($\alpha$-$Fe_2O_3$,$\gamma$- $Fe_2O_3$ and $Fe_3O_4$) are used in biomedicine as Magnetic Resonance Imaging contrast agents, vectors for drug delivery or agents for hyperthermia therapy [8, 9]. Iron oxides are also used as a material for magnetic storage media and in lithium-ion batteries [10-12]. Among the iron oxides, hematite ($\alpha$-$Fe_2O_3$) is the most common iron oxide in nature. $\alpha$-$Fe_2O_3$ is an n-type semiconductor, having a small band gap (2.1 eV) and is the most stable iron oxide under ambient conditions. Because of its small bang gap, hematite can absorb about 40% of the sunlight [13, 14] which is an important advantage for its use in solar energy conversion. In the last years many efforts have been focused on the obtaining methods of iron oxides. At present, iron oxide particles are synthesized by different methods such as the sono chemical route, co precipitation, solid state chemical reaction, hydrothermal methods, wood template, sol-gel and mechanical methods [15-21].

## 2. Material and method

### 2.1Chemical treatment of fiber

Ferric Nitrate ($Fe(NO_3)_3.9H_2O$) and ammonium chloride ($NH_4Cl$) was taken in the ratio 10:4 in 500 *ml* of distilled water. The mixture was stirred till a homogenous solution was obtained. In this mixture 10g of sisal fiber was added and then 1:1 solution of $NH_4OH$ (liquid ammonia) was added to it then left the solution for one hour. Again the mixture thus obtained was dried and then annealed in muffle furnace at 1000$^oC$ and kept it at different time duration sample 1 (SP1) for 15 min, sample 2 (SP2) for 30 min and sample 3 (SP3) for 45 min.

The reaction may take place in this way

$2Fe(NO_3)_3.9H_2O+3NH_4Cl+ 3NH_4OH$ + Fiber→ **$Fe_2O_3$: fiber** $+6NH_4NO_3 + 3HOCl + 18H_2O$

When ferric nitrate reacts with ammonium chloride and ammonium hydroxide along with sisal fiber at 1000$^oC$ with ammonium nitrate and HO-Cl (hypoclorous acid) decomposed at such high temperature and only **ferric oxide** is left.

### 2.2 Nature and structure of sample after firing

The material formed was found to in solid crystals in physical appearance. The sample appeared in powder form and it is like Cole in color.

**Result and discussion**

XRD

The amorphous state of the sisal fiber composite was verified by XRD. The x-ray diffraction patterns of $Fe_2O_3$ doped with sisal fiber shown in fig 1, 2 & 3. The peaks for $Fe_2O_3$ SP1 in fig 1 are observed at 2θ=10.744 (d=8.22775 Å), 2θ=24.164 (d=3.68020 Å), 2θ=33.190 (d=2.69705 Å), 2θ=35.663 (d=2.51552 Å), 2θ=40.913 (d=2.20401 Å), 2θ=49.508 (d=1.83965 Å), 2θ=54.127 (d=1.69305 Å), 2θ=57.717 (d=1.59599 Å), 2θ=62.497 (d=1.48491 Å), 2θ=64.067 (d=1.45226 Å) corresponding to (555), (562), (1032), (917), (611), (732), (713), (548), (649) and (648) reflections. The peaks present in $Fe_2O_3$ were also observed in the composition of sisal fiber with $Fe_2O_3$ which indicates the presence of ferrite particle. The entire pattern indicates about the small dimensions of the iron oxide particles. The changes in peaks occur due to the presence of composition of sisal fiber [22]. These radical cations through the coupling reaction lead to the ion of stable electrically conducting natural fiber. Reaction with the natural fiber generated by an internal redox reaction, which casus the reorganization of electronic structure to give the +ve and –ve nature of a radical is linked to its difference in reactivity towards lignin and cellulose/hemicelluloses [23].

ISSN:2319-6890)(online),2347-5013(print)
01 June 2015

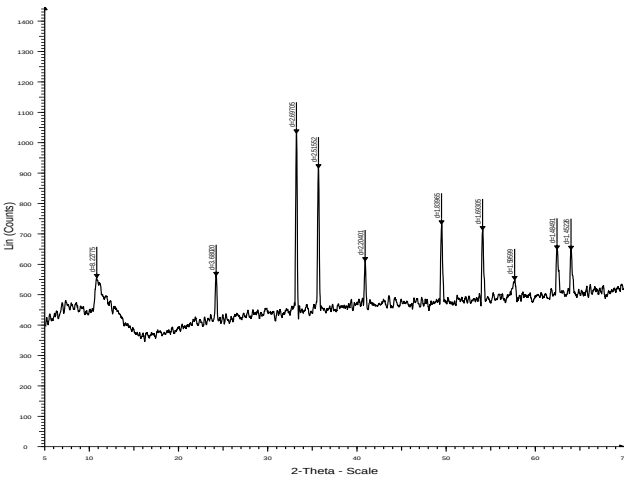


Fig 1

The peaks for $Fe_2O_3$ SP2 in fig 2 are observed at 2θ=25.285 (d=3.5194 Å), 2θ=29.540 (d=3.0214 Å), 2θ=34.845 (d=2.5726 Å), 2θ=37.460 (d=2.3988 Å), 2θ=43.025 (d=2.1006 Å), 2θ=52.2008 (d=1.7509 Å), 2θ=57.180 (d=1.6097 Å), 2θ=66.170 (d=14111 Å), 2θ=67.845 (d=1.3803 Å), 2θ=76.520 (d=1.2439 Å) corresponding to (914), (269), (1629), (930), (1980), (888), (1725), (936), (1161) and (289) reflections. The peaks present in $Fe_2O_3$ were also observed in the composition of sisal fiber with $Fe_2O_3$ which indicates the presence of ferrite particle and the peaks for $Fe_2O_3$ SP3 in fig 3 are observed at 2θ=25.330 (d=3.5133 Å), 2θ=34.890 (d=2.5694 Å), 2θ=37.505 (d=2.3960 Å), 2θ=43.075 (d=2.0982 Å), 2θ=52.225 (d=1.7489 Å), 2θ=57.225 (d=1.6085 Å), 2θ=61.000 (d=1.5177 Å), 2θ=66.220 (d=1.4101 Å), 2θ=67.220 (d=1.3794 Å), 2θ=76.585 (d=1.2430 Å) corresponding to (2296), (3887), (1915), (4481), (2112), (4019), (333), (1707), (2564) and (664) reflections. The peaks present in $Fe_2O_3$ were also observed in the composition of sisal fiber with $Fe_2O_3$ which indicates the presence of ferrite particle.

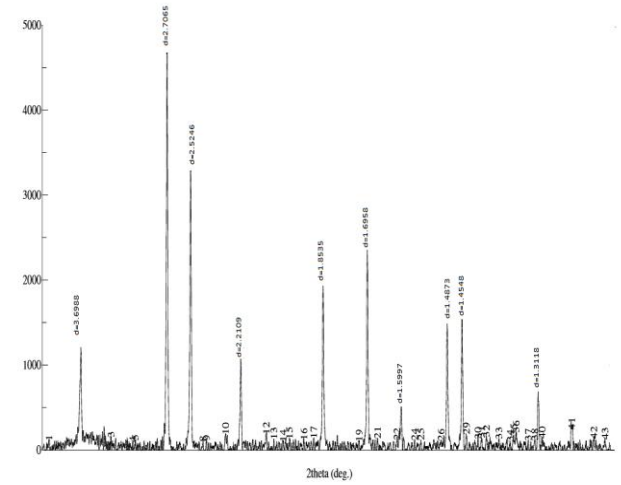


Fig 2

Natural sisal fiber consists of proton H+ molecule in its composition and deprotonation process is also occurred in natural fiber. Deprotonation is the removal of a proton (H+) from a molecule. Deprotonation of the radical cation is a major pathway and the proton removal decreases positive charge in the molecule and an increases negative charge. Deprotonation usually occurs from the donation of electrons or acceptance of the proton using a base, which forms its conjugate acid [24].

| Name | Symbol | Classification | A | B |
|---|---|---|---|---|
| Cellulose | $C_6H_{10}O_5$ | C-H Deprotonation | C | H |
| Hemi-celluloses | $C_5H_{10}O_5$ | C-H Deprotonation | C | H |
| Lignin | $C_{13}H_{34}O_{11}$ | C-H Deprotonation | C | H |

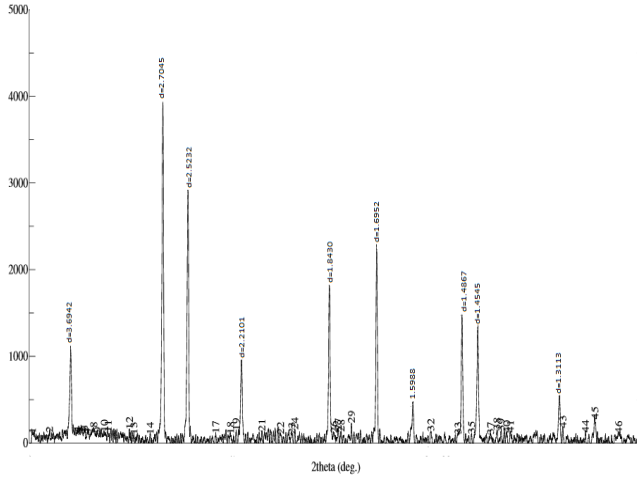


Fig 3

Some unknown peaks are present is the XRD graphs. Hence other crystalline phases such as various types of hydrated aluminum nitrate, ammonium chloride, sisal fiber or other impurities; might have been present in sample. Iron oxide cannot be produced at relatively very low temperature; therefore, it is not possible for nitrate ions to decompose. So that it's calcinated on high temperature at 1000°C the 2θ peaks (or miller indices) which indicates that $Al_2O_3$ was present. As the time increased from 15 min (SP1), 30 min (SP2) and 45 min (SP3), the intensity of Al2O3 phase peaks of SP2 increased as compare to SP1 and peaks of SP3 decreased as compare to SP2. The XRD results do not show that the sample was hydrated salt with other impurities. Therefore water molecules and impurities already removed at this temperature. After being calcinated at 1000°C the sample lost its crystalline structure and small amorphous humps appeared at 2θ= 8-12°, 33-38° and 53-64° for SP1; 2θ= 11-13°, 35-40° and 56-61° for SP2; 2θ= 11-12°, 36-45° and 55-60° for SP3. These humps are due to the interference of XRD signals of iron oxide. At this temperature Al2o3 phases lose their bonding and appear highly amorphous in nature its intensity of humps increased. These results indicate that at this temperature the iron oxide particles in several crystallize iron oxide. These finding was confirmed by referring to the XRD data base reference data base (KSD collection code 025778). The crystal system of the

ISSN:2319-6890)(online),2347-5013(print)
01 June 2015

structure was rhombohedral and had a density of 4.02cm$^{-3}$. The XRD peaks of SP2 and SP3 indicated the presence of α-iron oxide were at 2θ (miller indices) for SP2= 25.285, 29.540, 34.845, 43.025, 52.200, 57.180, 66.170, 67845, 76.520 and for SP3= 25.330, 34.890, 37.505, 43.075, 52.265, 57.225, 61.000, 66.220, 67.895, 76.585. Some of the reading has been verified due to impurities. The intensity of XRD peaks increased, indicating that more α-iron oxide crystals [25].

SEM

Figure 4, 5 & 6 (a) and (b) shows the morphology of $Fe_2O_3$. The micrograph depicts the crystalline nature. The variation in specular optical transmittance against wavelength for pure and doped iron oxide. This shows the typical micrograph of the clustering of well established randomly oriented nano rods which has compact, homogenous and well adherent growth onto the substrate. Fig (a) and (b) shows the morphology of material and fiber respectively. Fig (a) has porosity, non uniform and inside hollow texture. Its upper surface is in crystalline, non linear, soft and spongy form. In fig (b) fiber shows a crystalline, linear and smoky effect.

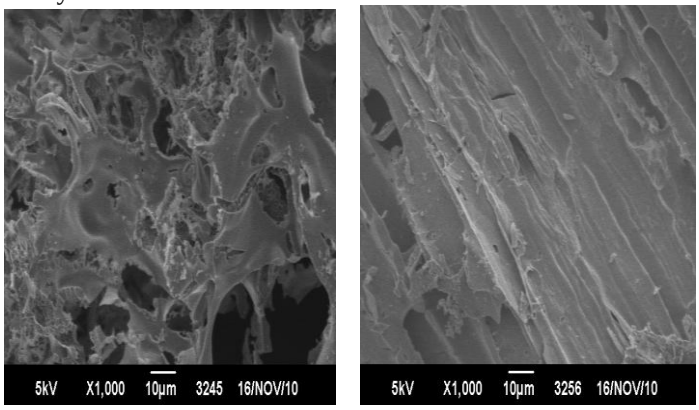


Fig 4

A change in the morphology and structure has been found after the treatment of sisal fibre which is confirmed by SEM technique. Figure 4, 5 & 6 shows the morphology of $Fe_2O_3$. The variations in specular optical transmittance against wavelength for pure and doped Aluminum oxide.

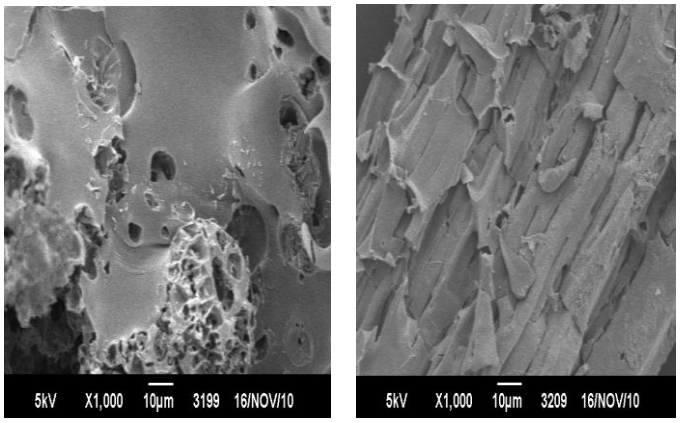


Fig 5

Uneven and cracked surface can be seen in the untreated samples which may be due to the presence of impurities in the fibre. The micrograph depicts the crystalline nature. This shows the typical micrograph of the clustering of well established randomly oriented nano rods which has compact, homogenous and well adherent growth onto the substrate.

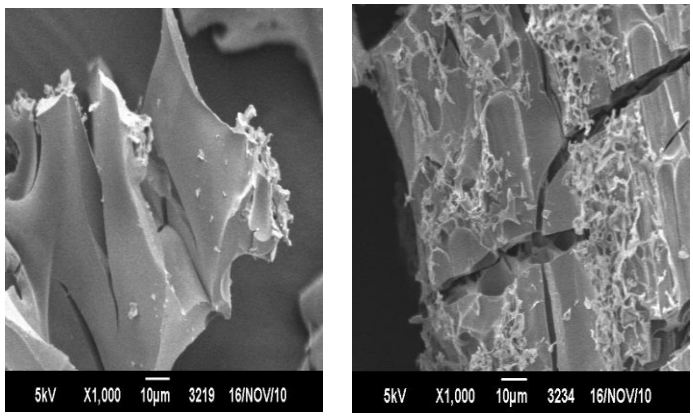


Fig 6

There was change in the unevenness of the surface in contrast of treated fibre it may be due to the chemical treatment done on the fibre. All images show the morphology of material and fiber respectively. Figures have porosity, non uniform and inside hollow texture.

TEM

Fig 7 (a) (b) and (c) for SP1, SP2 & SP3 respectively shows the non linear and non uniform dispersed iron oxide particles of 141.24nm and the agglomerated fiber containing 30.31-30.90mn size particles of iron oxide. The samples appear highly strained as seen in fig 7 (a) (b) and (c). The presence of dislocation loops is clearly seen. It is possible that the strain present in the sintered samples has a direct effect on the dielectric loss. The TEM micrographs show the heterogeneous microstructure iron oxides. A heterogeneous distribution of the individual phases is observed in all heterogeneous systems. On the other hand, in the iron oxide samples the particles possess needles like morphology with non-uniform sizes in a range from 141.31 to 30.90nm. These needles are less in numbers but large in size. The TEM investigations of the iron oxide composite samples show heterogeneous distribution with iron oxide needle like structure of about 30nm sizes. The diffraction pattern shows a higher grade of crystalline for the high iron oxide containing sample. The first fig shows the magnification 60000 which shows total palate of size of 141.31nm, second fig shows with the magnification of 80000 which is clearly shows the fibrous portion of the palate 30.31nm and third fig shows the magnification of 50000 which again shows the fibrous portion of the palate 30.90nm.

ISSN:2319-6890)(online),2347-5013(print)
01 June 2015

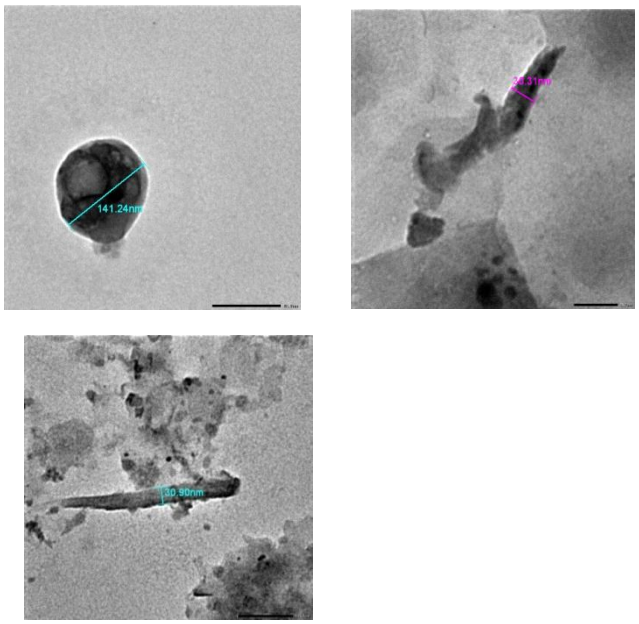


Fig 7 (a), (b) and (c)

The TEM graphs show the highly homogeneous microstructure if $Fe_2O_3$. $Fe_2O_3$ samples the ferric nitrate and ammonium chloride (10:4) one has still amorphous particles. The TEM investigations of the $Fe_2O_3$ composite samples show heterogeneous distribution with needle like structure. Among the sisal fiber doped iron samples with the composition has a longer amount of pores in the microspores region. Hence the pores size can be adjusted by the composition according to needs of the applications TEM observations confirmed the homogeneity of the microstructure. The morphology of the composites consists of iron oxide needles with high aspect ratio. It is possible to synthesize materials with different porosity features and surface morphology, which result in different applications by changing the ration of individual components in oxide system [26].

FTIR

The formation of α-$Fe_2O_3$ was approved by FTIR spectrum in figures showed that α-$Fe_2O_3$ is known to have spinal structures which exist over a range of hydrogen content captured by the empirical formula $H_{3m}Fe_{2-m}O_3$. It is clear that broad absorption bands appear at 3500-500$cm^{-1}$ respectively, which is attributed to the stretching vibration of hydroxyl groups. The peaks at 3127.07, 1399.42 and 584.57 $cm^{-1}$ correspond to the vibration of carboxylic acid groups. The IR transmission spectra of sisal fiber composite shown in fig from fig 8, 9 & 10 for SP1, SP2 & SP3 respectively were recorded in the range 500-4000 $cm^{-1}$. The wave number of fig 8 (SP1) 3127.0691, 2358.4974, 1641.0773, 1399.4211 and 584.5742$cm^{-1}$ shows the width 5546.5436, 2645.9742, 1986.4811, 855.5220 and 111.5815 $cm^{-1}$ of IR spectra respectively.

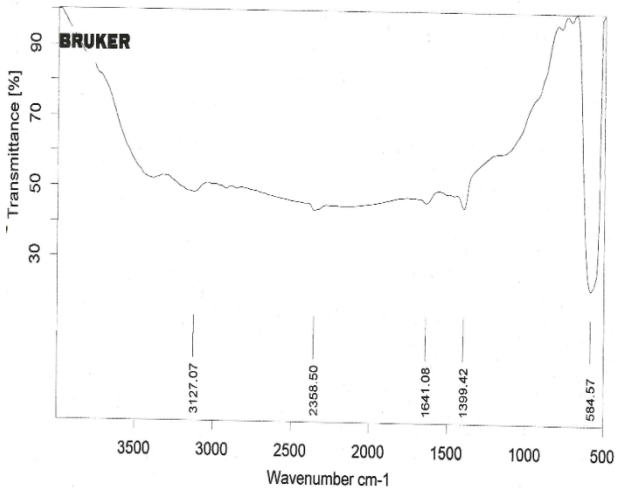


Fig 8

The prepared sample was free from visible inhomogeneities like cracks or bubbles. Decrease with a shifting of meta-center towards slightly higher wave number. For further increase of $Fe_2O_3$ the intensity of this band is continued to decrease where the first group of bands is also observed to decrease [27]. The peaks at 315.49, 1398.86 and 577.52 $cm^{-1}$ correspond to the vibration of carboxylic acid group. The wave number of fig 9 (SP2) 3125.4871, 2354.9447, 1638.8381, 1398.8550and 577.5146 $cm^{-1}$ shows the width 5546.5436, 2645.9742, 1986.4811, 855.5220 and 111.5815 $cm^{-1}$ of IR spectra respectively.

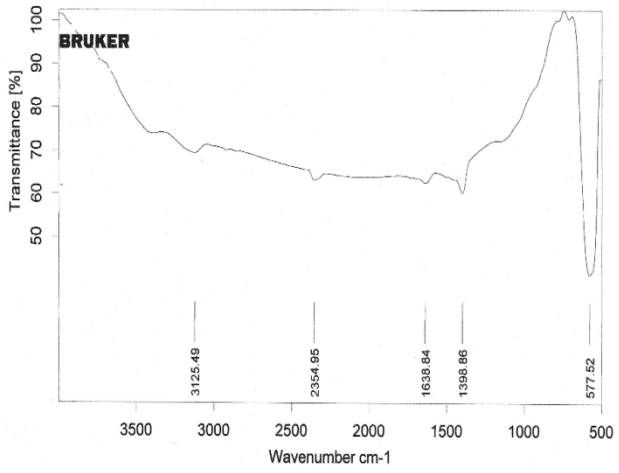


Fig 9

The peaks at 3120.86, 1397.32 and 556.55 $cm^{-1}$ correspond to the vibration of carboxylic acid group. The wave number of fig 10 (SP3) 3409.4926, 3120.82, 1633.1826, 1397.3193 and 5565486 $cm^{-1}$ shows the width 309.7282, 489.5764, 674.9217, 2712.0889 and 100.8427 $cm^{-1}$ of IR spectra respectively. The prepared sample was free from visible inhomogeneities like cracks or bubbles. Decrease with a shifting of meta-center towards slightly higher wave number. For further increase of

ISSN:2319-6890)(online),2347-5013(print)
01 June 2015

$Fe_2O_3$ the intensity of this band is continued to decrease where the first group of bands is also observed to decrease [27].

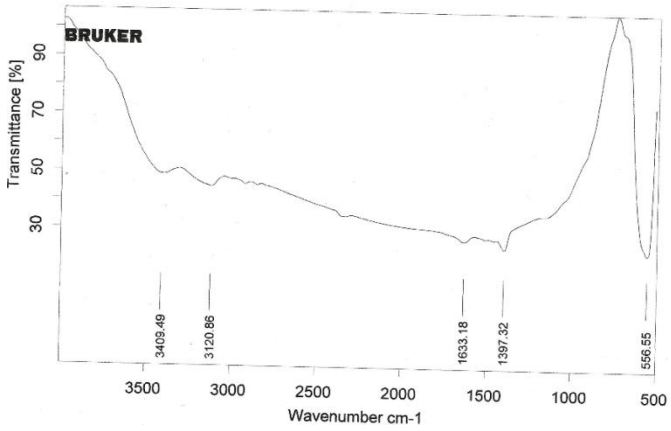


Fig 10

The stronger broadening bands 3500-1000 $cm^{-1}$for SP1, 3400-900 $cm^{-1}$ for SP2 and 3300-800 $cm^{-1}$for SP3 occurs due to the hydrogen bond between the various hydroxyl groups in the product. The stronger broadening bands 700-500 $cm^{-1}$ for SP1, SP2 & SP3 correspond to Fe-O vibration existed under the temperature of 1000°C at 15, 30 and 45 min for SP1, SP2 and SP3 respectively. In agreement with other works it is resulted that the main factor in obtaining of different iron oxide phases is the calcinations temperature at 1000°C leads to form the α-$Fe_2O_3$ [28].

Dielectrical measurement

The electrical properties of the insulating material $Fe_2O_3$ composite were measured by impedance analyzer these dielectric measurement of $Fe_2O_3$ composite doped with sisal fiber shown in fig 11 & 12for SP1, SP2 and SP3 respectively. In the Fig 11 represents the graph between frequency and tanδ and fig 12 shows the comparison between frequency and ε.

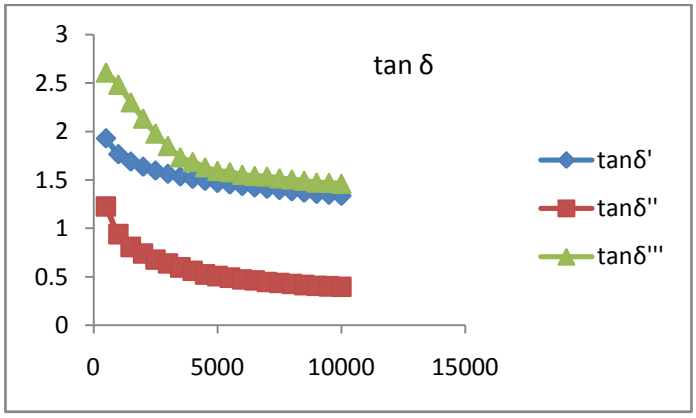


Fig 11

The dielectric constant ε and loss tanδ of $Fe_2O_3$ at room temperature 30°C are measured to be 1.9 to 1.3 respectively and are found to decrease with the increase in the frequency. The value of ε and tanδ are found to different with each other. In fig 11 the variation of dielectric constant at different frequencies with room temperature 30°C for $fe_2O_3$ is shows that it decreases considerably with increase in frequency. This dielectric dispersion is attributed to the Maxwell and Wagner type of interfacial polarization in agreement with Koop's phenomenological theory [29]. Since polarization decreases with increasing frequency and reaches constant values, a decrease in dielectric constant with frequency is observed.

At lower frequencies, dielectric loss tanδ is large and it decreases with increasing frequency. The tanδ is the energy dissipation in the dielectric system, which is proportional to the imaginary part of the dielectric constant. An increase in loss factor at higher frequencies may be due to the series resistance of the electrodes, leads, etc [30, 31].

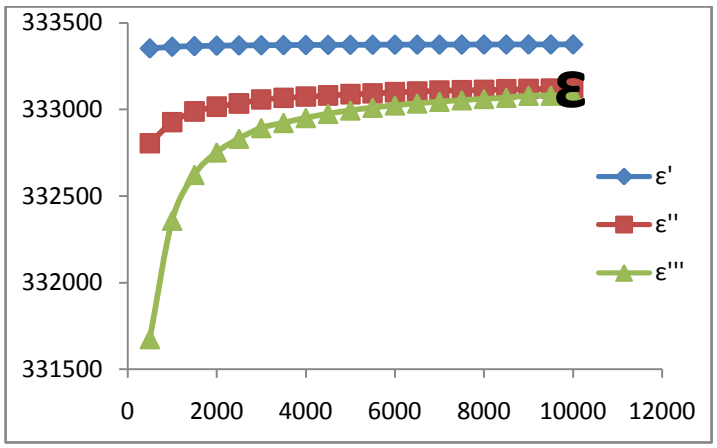


Fig 12

While in fig 12 is a comparison plot of variation of dielectric constant with different frequency at constant temperature shows an increase considerably with increase in frequency. It was observed from these figures that the dielectric constant increases continuously with increase in frequency for all the samples, followed with a frequency independent behavior. This is a normal behavior for high density, fine chemically homogeneous ferromagnetic material. The dielectric properties of ferrites are dependent upon several factors, including the method of preparation, chemical composition and grain structure, size and natural fiber (sisal fiber) and it's contains cellulose, hemicelluloses, lignin and pectin. The observed dielectric behavior of our samples may also be due to the particle size effect and is also in concurrence with observation made by other Investigators [32-34]. The effect of electrical homogeneity fine grain structure and shape of the ferrite samples affect the dielectric properties [35]. It also presence the α impurities contributes towards the change in dielectric properties. The dielectric constant of 25-30 at 10 KHz and an increasing trend is observed at higher frequencies. This is normal behavior for high density fine chemically homogenous ferromagnetic material [36]. The electronic exchange between ferrous and ferric ions didn't follow the path of frequency

ISSN:2319-6890)(online),2347-5013(print)
01 June 2015

which is externally applied alternating beyond the critical frequency value. The dielectric behavior of samples shown in graphs is because of its particle size effect [37]. If ε remains unaffected with increase in temperature then frequency also remains the same, which means that the local carriers are immobile. It is understood that the local charge carriers are immobile and the thermal activation in negligible. This further suggests that the samples possess a high chemical homogeneity and fine grain distribution. The presence of moisture, cellulose, hemicelluloses, lignin and pectin is also indicated by the electrical conductivity results. It is reported the presence of moisture plays an important role in the formation and stabilization of $Fe_2O_3$ [38].

## Conclusion

Calcinations of hydrated aluminum nitrate at high temperature eliminate steam, ammonium nitrate and dehydrate the aluminum nitrate and hypoclorous acid (volatile impurities). Calcinations dehydrate the aluminum nitrate salt and breakdown the nitrate ions at high temperature to produce α-iron oxide. Water molecules are released from the salt initially. Whereas other impurities released from salt at ~=1000$^o$C. The iron oxide is transformed to α-iron oxide after calcinations at temperature 1200$^o$C but because of sisal fiber and its impurities it converted in to α-iron oxide at temperature 1000$^o$C. The effect of chemical homogeneity, fine grain structure, particle size and shape of the ferrite samples are understood to affect the properties of dielectric behavior. The presence of moisture, cellulose, hemicelluloses, lignin and pectin also contribute towards changes in dielectric properties.

## References


i. *Son J. I., Kim H.J., Lee P. W., Role of Paper Sludge Particle Size and Extrusion; "Temperature on Performance of Paper Sludge Thermoplastic Polymer Composites"Journal of Appl. Polymer Sci., Vol. 82 (11), pp. 2709-2718, (2001).*

ii. *George J., Sreekala, M. S., Thomas S.," A Review on Interface Modification and Characterization of Natural Fiber Reinforced Plastic Composites", Polymer Engg. and Sci., Vol. 41, pp. 1471-1485, (2001).*

iii. *Karnani R., Krishnan M., Narayan R., "Biofiber-Reinforced Polypropylene Composites", Polymer Engg. and Sci., Vol. 37, pp. 476-483, (1997).*

iv. *Patil, D., Patil, V., Patil, P.: Sensors and Actuators B, vol. 152, 2011, p. 299*

v. *Zhang, F., Yang, H., Xie, X., Li, L., Zhang, L., Yu, J., Zha, H., Liu B.: Sensors and Actuators B, vol. 141, 2009, p. 381*

vi. *Liu, X., Liu, J., Chang, Z., Sun, X., Li, Y.: Catalysis Communications, vol. 12, 2011, p. 530*

vii. *Pailhé, N., Wattiaux, A., Gaudon, M., Demourgues, A.: Journal of Solid State Cemistry, vol. 181, 2008, p. 2697*

viii. *Dias, A., Hussain, A., Marcos, A., Roque, A.: Biotechnology Advances, vol. 29, 2011, p. 142*

ix. *Mahmoudi, M., Sant, S., Wang, B., Laurent, S., Sen, T.: Advanced Drug Delivery Reviews, vol. 63, 2011, p. 24*

x. *Srivastava, A., Ojha, A., Chaubey, S., Singh, J., Sharma, P.: Journal of Alloys and Compounds, vol. 500, 2010, p. 206*

xi. *Tartaj, P., Amarilla, JM.: Journal of Power Sources, vol. 196, 2011, p. 2164*

xii. *Hassan, MF., Rahman, MM., Guo, ZP., Chen, ZX., Liu, HK.: Electrochimica Acta, vol. 55, 2010, p. 5006*

xiii. *Penga, D., Beysena, S., Li, Q., Suna, Y., Yanga, L.: Particuology, vol. 8, 2010, p. 386*

xiv. *Boumaza, S., Boudjemaa, A., Omeiri, S., Bouarab, R., Bouguelia, A., Trari, M.: Solar Energy, vol. 84, 2010, p. 715*

xv. *Amir, HR., Vaezib, MR., Shokuhfarc, A., Rajabalic, Z.: Particuology, vol. 9, 2011, p. 95*

xvi. *Karami, H.: J Clust Sci, vol. 21, 2010, p. 11*

xvii. *Liang, HF., Wang, ZC.: Materials Letters, vol. 64, 2010, p. 2410*

xviii. *Ding, J., Fan, T., Zhanga, D., Saito, K., Guoa, Q.: Solid State Communications, vol. 151, 2011, p. 802*

xix. *Teja, AS., Koh, PY.: Progress in Crystal Growth and Characterization of Materials, vol. 55, 2009, p. 22*

xx. *Arbain, R., Othman, M., Palaniandy, S.: Minerals Engineering, vol. 24, 2011, p. 1*

xxi. *Roy, D., Deb, P., Basumallick, A., Basu, B.: J Opt, vol. 39, 2010, no.2, p. 102*

xxii. *s.k. dhawan kuldeep singh,anil,a.k. bakhshi polymeric & soft materials section. National physical laboratory. New delhi-110021. India*

xxiii. *ek et al. 1989*

xxiv. *Schmittle, M.; Burghart, A. Angew. Chem. int. Ed. EEngl.1997,36,2550.*

xxv. *Phase Transformations of α-Alumina Made from Waste Aluminum via a Precipitation Technique Khamirul Amin Matori, Loy Chee Wah, Mansor Hashim, Ismayadi Ismail and Mohd Hafiz Mohd Zaid Int. J. Mol. Sci.* ***2012****, 13(12), 16812-16821; doi:10.3390/ijms131216812*

xxvi. *W. Wunderlich, P. Padmaja, K.G.K. Warrier TEM characterization of sol-gel-processed alumina–silica and alumina–titania nano-hybrid oxide catalysts Journal of the European Ceramic Society 24 (2004) 313–317*

xxvii. *.S yusub, Gsahaya baskaranet al Indian journal of pure &applied physics Vol. 49 May 2011. Pp 315-322.*

xxviii. *Seyed Ali Hosseini, Aligholi Niaei, Dariush Salari Production of γ-Al2O3from Kaolin Open Journal of Physical Chemistry, 2011, 1, 23-27 doi:10.4236/ ojpc.2011. 12004 Published Online August 2011*

xxix. *Maxwell J C. Electricity and magnetism. London: Oxford University Press, 1993: 828*

xxx. *Sawant V S, Shinde S S, Deokate R J, et al. Effect of calcining temperature on electrical and dielectric properties of cadmium stannate. Appl Surf Sci, 2009, 255: 6675*

xxxi. *Babar A R, Shinde S S, Moholkar A V, et al. Electrical and dielectric properties of co-precipitated nanocrystalline tin oxide. J Alloys Compd, 2010, 505: 743*

xxxii. *Goswami A, Goswami A P. Dielectric and optical properties of ZnS films. Thin Solid Films, 1973, 16: 175*

xxxiii. *J. Volger, Philips tech. Rdsch. 22, 306 (1960/61*

xxxiv. *Das and Pramanik 1998; Rane etal2001*

xxxv. *Murthy 1990*

xxxvi. *Katsumi etal1975*

xxxvii. *Vijay a hiremath and A Venkataraman 2002*

xxxviii. *Rehman and Venkataraman 2002*